Sakarya Üniversitesi Fen Bilimleri Dergisi
Sakarya University Journal of Science

ISSN : 2147-835X
Publisher : Sakarya University

Vol. 29, No. 1, 125-139, 2025
DOI: https://doi.org/10.16984/saufenbilder.1589238

Research Article

Air-Exposure-Driven Color and Optical Variations in Hydroxyapatite Extracted from Fish Scales

H. Esma Okur

Bursa Technical University, Faculty of Engineering and Natural Sciences, Department of Chemistry, Bursa, Türkiye, esma.okur@btu.edu.tr

ARTICLE INFO

Keywords:
Hydroxyapatite
Fish scales
Band gap
Air exposure
Rietveld refinement

Article History:
Received: 21.11.2024
Revised: 21.02.2025
Accepted: 25.02.2025
Online Available: 28.02.2025

ABSTRACT

The disposal of fish scales as waste presents an environmental challenge and an untapped opportunity for resource recovery. In this study, hydroxyapatite (HAp) was extracted from European seabass (Dicentrarchus labrax) scales to explore how air exposure during calcination affects its optical and surface properties. HAp powders were prepared under two distinct calcination conditions: fully exposed to air (producing white powder) and partially shielded from air (resulting in gray powder). Rietveld refinement of X-ray powder diffraction (XRPD) data confirms that both powders crystallize in the hexagonal HAp structure, with a minor Mg-whitlockite impurity. Despite these differences in air exposure, the bulk structure of the HAp remains unchanged. The color variations are linked to surface oxidation, as subsurface layers in the partially shielded scales retain a grayish tone while the exposed surfaces turn completely white. Scanning electron microscopy reveals subtle differences in particle morphology: the white powder had a smoother surface compared to the slightly rougher gray powder. Fourier transform infrared spectra confirm the presence of characteristic phosphate and hydroxyl groups in both powders, indicating that the core chemical structure of HAp is intact in both cases. The Ca/P ratios—1.504(7) for the white powder and 1.505(7) for the gray powder obtained from the Rietveld analysis—further support the stoichiometric integrity of the material. UV-Vis spectroscopy reveals direct bandgap values of 3.99 eV for the white powder and 3.87 eV for the gray powder. These bandgap values, which are lower than those typically reported for defect-free HAp (5–6 eV), suggest that the optical differences between the powders are driven by surface effects, such as oxygen vacancies or trace impurities. This study highlights how calcination conditions, particularly air exposure, influence surface properties and optical behavior, paving the way for potential applications of fish-scale-derived HAp in electronic and optical materials.

1. Introduction

Hydroxyapatite (HAp) is a calcium phosphate mineral composed of calcium cations (Ca^{2+}), orthophosphate (PO_4^{3-}), and hydroxide (OH^-) ions, with a stoichiometric formula of $Ca_{10}(PO_4)_6(OH)_2$, resulting in a calcium-to-phosphorus ratio (Ca/P) of 1.67. HAp is widely regarded as one of the most valuable bioceramic materials due to its close structural similarity to natural bone, where the inorganic component consists of approximately 60 wt% HAp. Therefore, since the 1980s, HAp has gained widespread recognition for its exceptional chemical stability and biocompatibility, making it a prominent material in dental and orthopedic applications [1–5].

HAp is known to exist in two crystallographic structures: the hexagonal (space group $P6_3/m$) [6] and monoclinic crystal systems (space group $P2_1/b$) [7], with subtle differences in atomic arrangement, particularly in the orientation of the hydroxyl groups, while both

Cite as: H. E. Okur (2025). Air-Exposure-Driven Color and Optical Variations in Hydroxyapatite Extracted from Fish Scales, *Sakarya University Journal of Science*, 29(1), 125-139. https://doi.org/10.16984/saufenbilder.1589238

maintain a Ca/P ratio of 1.67. In the hexagonal structure, the hydroxyl groups are oppositely oriented. However, in the monoclinic structure, the hydroxyl groups are oriented in the same direction within the same column but are oppositely oriented between columns [8]. Therefore, accurate structural determination is crucial for specific applications.

Synthetic methods are commonly employed to produce HAp [9], as they offer a controlled process that minimizes the risk of defects, impurities, vacancies, and deficiencies. However, there is growing interest in extracting HAp from natural sources [10, 11], such as fish scales, which are a by-product of the seafood industry. The use of fish scales in the production of an important bioceramic material like HAp holds significant value for sustainability.

Additionally, recycling this by-product, which would otherwise be considered waste, plays a crucial role in reducing environmental impact.
As a result, there has been growing interest in optimization of the extraction of HAp from natural sources to minimize structural anomalies such as defects, cation or anion deficiencies, or deviations from stoichiometry. It is well known that biological apatites often deviate from the stoichiometric composition of HAp and contain some amount of ion substitutions, including Na^+, Mg^{2+}, K^+, HPO_4^{2-}, CO_3^{2-}, Cl^-, and F^- [12]. It is therefore crucial to extract HAp free from the aforementioned structural anomalies, as defects, vacancies, and deficiencies significantly impact the electronic and optical properties of HAp. For instance, recent studies have applied various pre-treatment methods to examine the morphological and structural characteristics of HAp derived from fish scales. One such study found that boiling the scales prior to calcination significantly impacted the morphology and crystallinity of the extracted HAp powder [13].

Fish scales that were boiled before calcination produced spherical particles at higher temperatures, while non-boiled scales led to the formation of nanorods, underscoring the major influence of pre-treatment on microstructure and potential defect formation. Notably, the study also reported differences in color between the boiled and non-boiled samples, indicating that the pre-treatment affected not only the structure but also the appearance of the HAp powder [13]. This underscores the importance of the extraction method in determining the structural properties of HAp, which ultimately has a significant effect on the electronic properties of material.

A recent study by Okur [14] further contributed to this field by employing a straightforward yet effective calcination method to extract HAp from recycled European seabass scales. In that work, the scales were calcined at 800 °C, resulting in the formation of highly crystalline HAp with minimal secondary phases, as verified by Rietveld refinement of X-ray powder diffraction data. Magnesium whitlockite was identified as a minor impurity, which may be beneficial for biomedical applications owing to its positive influence on bioactivity and osteoconductivity. In addition, HAp was incorporated into polyvinyl alcohol composite films, demonstrating improved adsorption efficiency for methylene blue dye and underscoring the material's potential for environmental remediation. Building on these findings, the same calcination parameters (800 °C for 2 hours) were applied in the present study to systematically examine the influence of air exposure on the surface and optical properties of HAp, while minimizing additional confounding factors.

In addition to the structural studies, numerous theoretical and experimental studies have been conducted to uncover the electronic and optical properties of HAp considering the defect levels, vacancies, *etc.* [15–21]. Unfortunately, due to the lack of accurate structural characterization and/or poor sample quality, it has been challenging to elucidate fundamental properties such as the electronic band structure and band gap. This has led to significant discrepancies in the obtained values, especially for the band gap. For instance, the measured width of the forbidden electronic gap (E_g) ranges from above 6 eV down to 3.95 eV.

Recent investigations have shed light on how the optical and electronic properties of HAp influence its bioactivity and broader applications. Rosenman et al. [15] demonstrated that HAp possesses distinct bulk and surface-localized electron-hole states, as revealed by

photoluminescence (PL) and surface photovoltage spectroscopy (SPS). Their findings suggest that these deep electron-hole charged states may contribute to enhanced cell attachment, bone regeneration, and overall biocompatibility. Avakyan et al. [19] later explored how oxygen vacancies and structural defects impact the electronic structure and optical absorption of HAp, indicating that processing conditions and surface modifications can be instrumental in tuning these properties.

Computational studies have also provided valuable insights into the influence of defects on HAp behavior. Bystrov et al. [22] examined oxygen and hydroxyl vacancies as well as atomic substitutions, showing that such defects alter the band structure, optical transparency, and mechanical stability of HAp. Their work highlights how oxygen-related defects in particular can create localized electronic states within the bandgap, thus affecting the material's electronic response. In an earlier study, Bystrov et al. [23] used first-principles calculations to investigate various defect types—including oxygen and hydroxyl vacancies, cation substitutions, and interstitials—and their effects on the density of electronic states (DOS) and bandgap. These modifications introduce additional energy levels in the forbidden zone, which may prove beneficial for biomedical coatings, implant materials, and nanomedical applications.

Rial et al. [24] further underscored the versatility of nanosized HAp for environmental remediation, catalysis, and drug delivery, where the electronic surface properties play a key role. Collectively, these studies illustrate that the optical and electronic properties of HAp are not merely static material characteristics; rather, they can be actively tailored through defect engineering, synthesis conditions, and doping strategies to support a range of applications. As research progresses, the potential for HAp in optoelectronics, bioactive materials, and environmental technologies continues to expand, making detailed knowledge of its band structure more relevant than ever.

This study focuses on a detail that has not been addressed in previous research on the extraction of HAp from fish scales. It offers a new perspective by investigating the effects of both pre-treatments before calcination and the level of air exposure during calcination. In this process, the fish scales were boiled in water before calcination to remove organic matter. Subsequently, two different calcination methods were employed: in the first scenario, each fish scale was in direct contact with air inside the furnace, while in the second scenario, only the surface scales were in direct contact with air, and the scales beneath the surface were shielded from air exposure by the top layer.

In other words, the first group was fully exposed to air, while the second group underwent calcination as partially shielded beneath the surface. After calcination, it was observed that the fully exposed fish scales on the surface were completely white, whereas the partially shielded scales beneath the surface were white-gray/black in color. After grinding the calcined fish scales, white and gray HAp powders were obtained. The main objective of this research is then to investigate how different calcination environments influence the formation of HAp, focusing on the resulting color, optical and structural differences between the white powder, produced from fully exposed scales, and the gray powder, obtained from partially shielded scales.

The structural characterisation was performed through Rietveld refinement of X-ray powder diffraction (XRPD) data, Fourier transform infrared spectroscopy (FTIR), and scanning electron microscopy (SEM). Additionally, UV-Vis spectroscopy was used to examine the optical properties of both samples, specifically to understand how varying air exposure during calcination affects the band gap and light absorption. This study delves deeper into the mechanisms of HAp formation from fish scales, while also examining how different calcination conditions affect its structural and optical properties. These insights are valuable for applications where natural HAp's color and structural integrity play key roles.

2. Materials and Methods

2.1. Preparation of hydroxyapatite powder from European seabass (Dicentrarchus labrax) scales

Scales from European seabass (Dicentrarchus labrax), sourced as a by-product from Bursa Kocamanlar Seafood. The same batch of fish scales used in [14] was employed here, where the detailed structural characterization of the raw scales is documented. Relevant information can be found in the Electronic Supplementary Information (ESI) of [14]. The choice of calcination temperature (800 °C) and duration (2 hours), with a heating rate of 10 °C/min, was based on thermogravimetric analysis results presented in [14].

Two groups of calcined samples were prepared: one in which the scales were placed in a single layer for full air exposure, and another in which the scales were stacked, reducing air contact for inner layers. This straightforward yet controlled arrangement ensures repeatable differences in oxidation and thermal decomposition between the two groups.

Prior to calcination, the scales were boiled in deionized water for 4 hours to remove organic matter and collagen. They were then filtered and allowed to dry in a fume hood for 24 hours. Once dry, the scales were divided into two groups. In the *fully exposed* group, the scales were arranged in a single layer to maximize air contact during calcination. In the *partially shielded* group, the scales were stacked so that inner layers were covered by surface scales, reducing their direct exposure to air. Both groups were calcined at 800 °C for 2 hours with a heating rate of 10 °C/min, as specified in [14].

Following calcination, the fully exposed group turned completely white, while the partially shielded group exhibited both white and gray regions (Figure 1). In both groups, the outermost (surface) scales remained white. After cooling to room temperature, the scales were initially ground using a coffee grinder and then further reduced in size with a mortar and pestle. The resulting white powder (from fully exposed scales) and gray powder (from partially shielded scales) were sieved through a 150 µm sieve and stored for subsequent analyses.

2.2. Structural characterisation

2.2.1. X-ray powder diffraction (XRPD)

X-ray powder diffraction (XRPD) measurements were conducted using a Bruker D8 Advance diffractometer in Bragg-Brentano geometry. Data were collected at room temperature over an angular range of $2\theta = 5-60°$, with a step size of 0.02°, utilizing Cu Kα radiation ($\lambda = 1.54056$ Å). The collected XRPD data were analyzed through Rietveld refinement, employing the General Structure Analysis System (GSAS), a widely used software suite written in FORTRAN [25]. Throughout the refinement process, various key factors were carefully optimized, such as peak intensities, background fitting, and lattice parameters, to ensure accurate results.

The quality of the refinement was evaluated through *R*-factors, including the weighted profile *R*-factor (R_{wp}) and the expected statistical *R*-factor (R_{exp}), with the goodness-of-fit determined by the χ^2 value. A pseudo-Voigt function [26], which combines Gaussian and Lorentzian components, was used to model the peak shapes, while the background was fitted using a Chebyshev polynomial function. Anomalous X-ray scattering factors, such as corrections to form factors (f' and f''), were computed with the DISPANO program [27] and incorporated into the GSAS refinement. The iterative refinement cycles included adjustments to profile shape parameters, zero-point corrections, background modeling, and scale factors, along with atomic thermal displacement parameters for the phases analyzed.

Figure 1. Schematic representation of hydroxyapatite (HAp) powder preparation from European seabass scales. The top image shows the cleaned fish scales after removing dirt and debris. The central image depicts the scales after boiling for 4 hours and drying in a fume hood for 24 hours. The left image shows the gray powder obtained from partially shielded scales, where inner scales were shielded from air exposure during calcination. On the right is the white powder, derived from fully exposed scales calcined in a single layer, allowing full air exposure. The bottom images show the final powders after grinding, highlighting the distinct color differences between the gray and white powders

2.2.2. Fourier transform infrared spectroscopy (FTIR), scanning electron microscopy (SEM) and UV-Visible spectroscopy

The functional groups in the extracted powders were identified using a Fourier transform infrared (FTIR) spectrometer equipped with an Attenuated Total Reflectance (ATR) diamond probe. Spectra were collected over the range of 4000–400 cm^{-1} on a Thermo Nicolet iS50 FTIR system. For morphological analysis, scanning electron microscopy (SEM) was performed using a Zeiss Gemini 300 microscope with a Bruker XFlash 6I100 detector in In-Lens mode. Prior to imaging, the samples were coated with a thin layer of gold-palladium (Au-Pd) alloy (60:40 ratio), applying a 15 nm conductive coating using a Leica EM ACE600 high-vacuum sputter coater to enhance surface conductivity. Optical absorbance measurements of the powders, across the wavelength range of 200–800 nm, were conducted using an Agilent Cary 60 UV-Vis spectrophotometer.

3. Results

3.1. Rietveld analysis

Ambient temperature XRPD data for the fully exposed white and partially shielded gray powders confirmed the successful extraction of crystalline hydroxyapatite, HAp, from fish scales, as shown in Figure 2**.** The figure highlights the crystalline similarity between the two samples: white HAp powder (fully exposed to air), gray HAp powder (partially shielded). Minor variations in peak intensities are observed, but no significant differences in overall crystallinity are present.

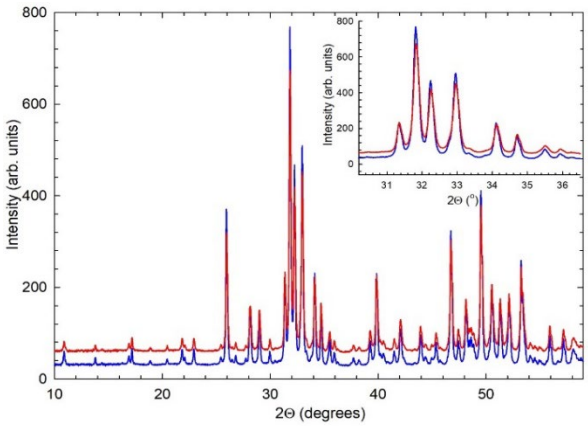

Figure 2. X-ray powder diffraction (XRPD) patterns of hydroxyapatite (HAp) extracted from the fish scales collected at ambient temperature with λ = 1.5406 Å. The red curve represents the white powder (fully exposed) the blue curve corresponds to the gray powder (partially shielded). The inset shows a magnified view of the 2θ = 30.2–36.5°, emphasizing the crystalline similarity among the samples, with minor differences in peak intensities

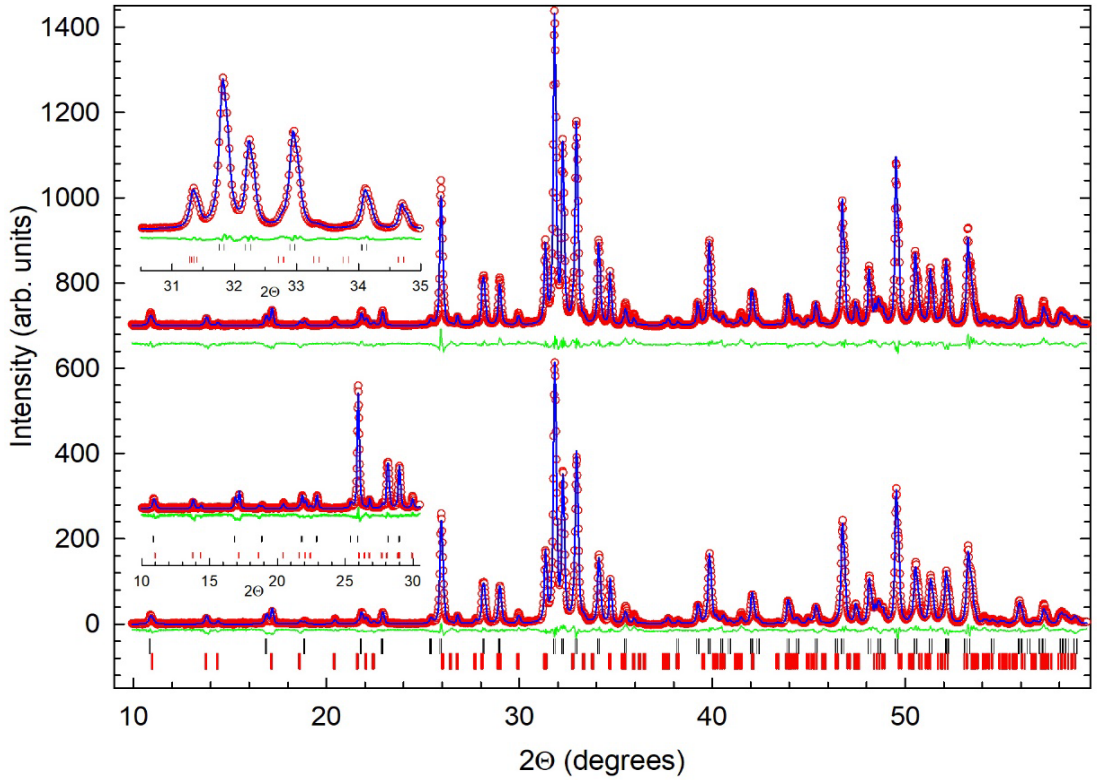

Figure 3. Rietveld fits to XRPD data for the gray (partially shielded, upper profile) and white (fully exposed, lower profile) hydroxyapatite (HAp) powders collected at ambient temperature with λ = 1.5406 Å. The red circles represent the observed data, blue lines the calculated profile, and green lines the difference between observed and calculated profiles. Black and red ticks mark the reflection positions of the majority phase hexagonal HAp $Ca_{10}(PO_4)_6(OH)_2$ (space group $P6_3/m$) and minority rhombohedral Mg-Whitlockite $Ca_{18}Mg_2H_2(P0_4)_{14}$ (space group $R3c$), respectively. The weighted-profile and expected R-factors for the upper fit are R_{wp} = 4.54% and R_{exp} = 1.15% while for the lower fit they are R_{wp} = 3.88% and R_{exp} = 1.13%. The insets highlight different 2θ regions of the corresponding profiles, emphasizing the peak fitting and the contribution of the secondary Mg-Whitlockite phase

The Rietveld refinement (Figure 3) reveals that both the white and gray powders crystallize in the hexagonal space group $P6_3/m$ (no. 176) [28], along with a secondary phase, identified as magnesium whitlockite ($Ca_{18}Mg_2H_2(PO_4)_{14}$) as in the previous study [14]. This impurity is modeled using the rhombohedral space group $R3c$ (no. 161) [29]. Previous studies on extracting HAp from natural sources using calcination have commonly reported the formation of HAp in a hexagonal structure, consistent with the findings of this study. However, these works often identified β-tricalcium phosphate (β-TCP, $Ca_3(PO_4)_2$) as the secondary phase, typically without employing detailed Rietveld refinement [13, 30, 31]. The similarity in the chemical composition and crystal structure of β-TCP and whitlockite (WH) frequently leads to their confusion in discussions regarding calcium phosphate phases [29]. Both minerals share the same space group ($R3c$) but have distinct unit cell parameters, making them difficult to differentiate through standard XRPD analysis, especially as their Bragg reflections can overlap.

Magnesium incorporation into whitlockite causes slight distortions in the crystal lattice, resulting in subtle variations in bond lengths, angles, and the overall structural stability compared to pure β-TCP. The f' and f'' corrections applied in GSAS were: Ca (f' = 0.340, f'' = 1.235), P (f' = 0.283, f'' = 0.433), Mg (f' = 0.165, f'' = 0.177), and O (f' = 0.046, f'' = 0.032). The refined unit cell parameters, P–O bond lengths, and weight fractions of HAp and WH phases for both the white and gray powders are summarized in Table 1.

The unit cell parameters for both phases – $a = b$ = 9.4235(1) Å, c = 6.8800(1) Å for the white powder, and $a = b$ = 9.4232(1) Å, c = 6.8806(1) Å for the gray powder – are nearly identical within experimental uncertainty, despite the color differences. These values are consistent

with previously reported data [14]. Similarly, the weight fractions of HAp (83.27(3) wt% for the white and 83.57(3) wt% for the gray) and Mg-whitlockite (16.7(1) wt% for the white and 16.4(1) wt% for the gray) phases show no notable differences between the fully exposed and partially shielded powders. Additionally, the P–O bond lengths in the HAp structure are virtually identical for both powders, with minimal variation within experimental error.

Table 1. Refined structural parameters and weight fractions of the major hydroxyapatite and minor Mg-Whitlockite phases present in the white and gray powders obtained from the fully exposed and partially shielded region of the fish scales

	structural parameters	white – fully exposed	gray – partially shielded
Hydroxyapatite ($P6_3/m$)	$a = b$ (Å)	9.4235(1)	9.4232(1)
	c (Å)	6.8800(1)	6.8806(1)
	V (Å^3)	529.106(9)	529.120(8)
	P−O1 (Å)	1.577(4)	1.575(4)
	P−O2 (Å)	1.536(4)	1.529(4)
	P−O3 (Å)	1.631(2)	1.625(2)
	weight fraction (%)	83.27(3)	83.57(3)
Mg-Whitlockite ($R3c$)	$a = b$ (Å)	10.3474(3)	10.3474(3)
	c (Å)	37.084(2)	37.079(2)
	V (Å^3)	3438.7(2)	3438.1(2)
	weight fraction (%)	16.7(1)%	16.4(1)

Table 2. Refined structural parameters for hexagonal biogenic hydroxyapatite (space group $P6_3/m$) from Rietveld analysis of XRPD data collected at ambient temperature from the partially exposed gray (upper) and fully exposed white (lower) powders, at room temperature with λ = 1.5406 Å. Site multiplicities and ocuupancies are listed in columns *M and N,* respectively. Values in parentheses are estimated errors from the least-squares fitting. The weighted-profile and expected *R*-factors for the white and gray powders are R_{wp} = 3.88%, R_{exp} = 1.13% and R_{wp} = 4.54%, R_{exp} = 1.15%, respectively

Atoms	*x/a*	*y/b*	*z/c*	*M*	*N*
Ca(1)	0.3333	0.6667	0.0017(5)	4	0.998(3)
Ca(2)	0.25572(24)	0.99784(27)	0.25	6	0.963(6)
P	0.4015(4)	0.35716(33)	0.25	6	1.082(4)
O(1)	0.3404(5)	0.4850(5)	0.25	6	1
O(2)	0.5868(5)	0.4748(10)	0.25	6	1
O(3)	0.3394(4)	0.2430(4)	0.0566(4)	12	1
O-h	0	0	0.19500	4	0.5
H	0	0	0.06080	4	0.5
Atoms	*x/a*	*y/b*	*z/c*	*M*	*N*
Ca(1)	0.3333	0.6667	0.0014(5)	4	0.999(3)
Ca(2)	0.25537(23)	0.99740(27)	0.25	6	0.963(3)
P	0.40203(32)	0.35686(32)	0.25	6	1.083(4)
O(1)	0.3415(5)	0.4855(5)	0.25	6	1
O(2)	0.5881(5)	0.4744(9)	0.25	6	1
O(3)	0.3408(4)	0.2433(4)	0.0553(4)	12	1
O-h	0	0	0.19500	4	0.5
H	0	0	0.06080	4	0.5

The refinement of the site occupancies of the Ca(1), Ca(2), and P atoms for the white and gray powders yielded stoichiometric values of Ca:P = 9.77(2): 6.50(3) yielding Ca/P: 1.504(7) and

Ca:P = 9.77(2): 6.49(3) yielding Ca/P: 1.505(7), respectively. Although these values fall below the ideal Ca/P ratio of 1.67 for stoichiometric HAp, such deviations are typical of biogenic HAp owing to ionic substitutions [10, 11].

In a previous study, the Ca/P ratio for HAp derived from the same fish scales was refined as 1.474(7), reinforcing the notion that naturally sourced HAp often exhibits a Ca-deficient profile. Crucially, the Ca/P ratios remain similar for both the fully exposed (white) and partially shielded (gray) powders. It should be noted that, during the refinement process, the P–O bond lengths were constrained to 1.55 Å [28] due to the limitations of X-rays in accurately determining the positions of light elements.
The fractional atomic coordinates of P, O(1), O(2), and O(3) were refined with a tolerance of 0.05 and a bond length restraint weight of 100 (presented in Table 2). Variations in air exposure during calcination do not significantly alter the fundamental structural characteristics of the extracted HAp. Full air exposure primarily affects the surface, leading to color changes likely caused by surface oxidation or the interaction of trace impurities with an oxygen-rich environment. These surface effects, potentially creating oxygen vacancies or defects, modify the electronic structure, contributing to the color differences observed.

However, these modifications remain confined to the surface, leaving the bulk crystal structure unaffected. Additionally, the consistent Ca/P ratios across the fully exposed (white) and partially shielded (gray) powders confirm that air exposure does not influence the stoichiometry of the calcium and phosphorus atoms. This indicates that the observed color changes due to air exposure are limited to surface properties and do not impact the bulk structure or stoichiometric composition of the HAp.

3.2. FTIR analysis

The FTIR spectra shown in Figure 4 confirm the presence of key functional groups characteristic of HAp. The observed bands correspond to distinct infrared absorption modes of the free orthophosphate ion (PO_4^{3-}), which has nine degrees of freedom that simplify into four normal modes of vibration. The ν_1 mode, associated with P–O symmetric stretching, is detected around 964 cm^{-1}, confirming the presence of the HAp phase, consistent with previously reported values [32]. The ν_3 mode, attributed to the antisymmetric P–O stretching, appears as bands at 1088, 1030, and 980 cm^{-1}, representing triply degenerate stretching vibrations. The ν_4 mode, corresponding to antisymmetric P–O bending, is identified by the bands at 600 and 565 cm^{-1}, typical of HAp.

Additionally, the OH^- group is characterized by a distinct band around 3600 cm^{-1}, indicating the stretching vibrations of the O–H bond, while the band near 630 cm^{-1} corresponds to the librational motion of the OH^- ion [13], a feature specific to HAp and absent in related phases such as fluorapatite and chlorapatite [32]. These spectra confirm the successful formation of HAp in both the fully exposed and partially shielded samples, While the characteristic bands for the PO_4^{3-} groups are consistent across both samples, slight differences in intensity are observed.

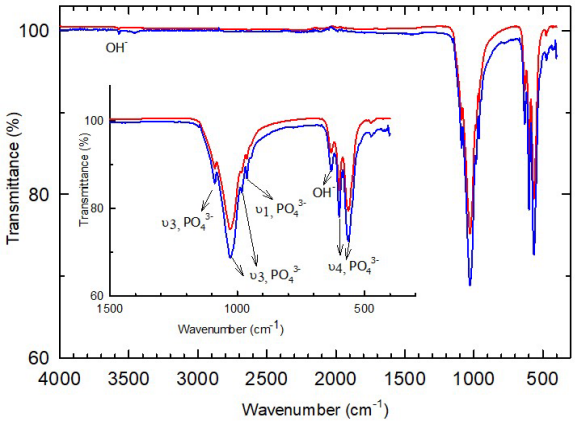

Figure 4. FTIR spectra of the hydroxyapatite (HAp) powders. The red spectrum represents the white HAp powder (fully exposed), while the blue spectrum represents the gray HAp powder (partially shielded). The labeled bands correspond to characteristic functional groups, with further details provided in the main text. The inset shows an expanded view of the wavenumber range 1500–300 cm^{-1}, focusing on the absorption modes of the PO_4^{3-} groups in HAp, which are labeled and indicated by arrows

3.3. SEM analysis

The SEM images in Figure 5 provide a morphological analysis of the white and gray HAp powders, revealing variations in particle

shape, crystallite size, and degree of surface crystallization. At lower magnifications (Figures 5a and 5c), both powders exhibit aggregated particles, though the gray powder shows more pronounced irregularities in particle shape compared to the smoother, more uniform appearance of the white powder. At higher magnifications (Figures 5b and 5d), individual HAp particles, ranging from approximately 45 nm to 135 nm in size, are observed in both powders, confirming the nanoscale nature of the crystallites. Observed differences in particle morphology and surface texture may result from variations in air exposure during calcination, with the fully exposed white powder showing a more uniform and smoother surface. The presence of nanoscale crystallites in both powders indicates the potential for increased surface area, which could be advantageous for applications requiring high surface interactions, such as adsorption or various biomedical uses.

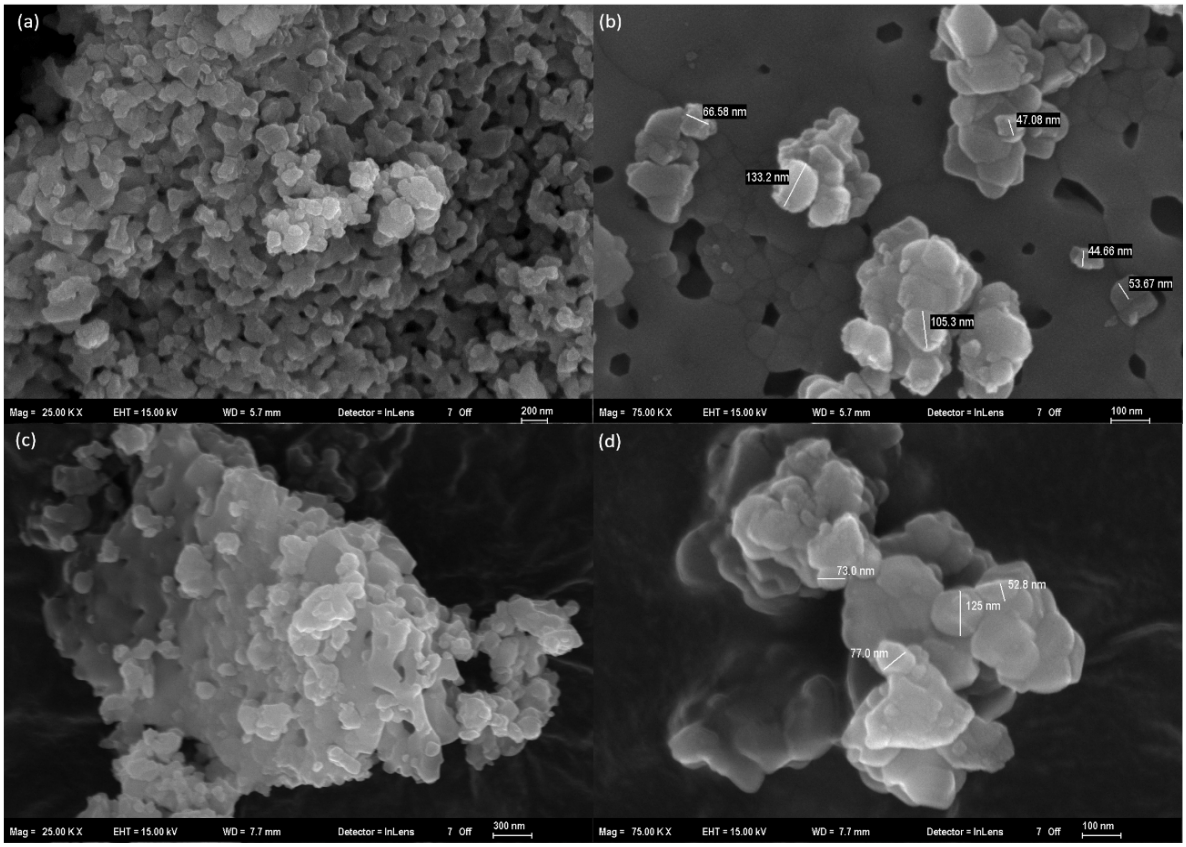

Figure 5. SEM images of hydroxyapatite (HAp) powders extracted from fish scales, comparing white (fully exposed, upper panels) and gray (partially shielded, lower panels) powders at different magnifications. (a, c): Low-magnification (25.0 kX) overviews of the white (a) and gray (c) powders. (b, d): High-magnification (75.0 kX) close-ups of the white (b) and gray (d) powders, highlighting individual HAp crystallites ranging in size from approximately 45 nm to 135 nm

3.4. UV-Vis spectroscopy

The optical properties of the white and gray HAp powders were analyzed using UV-Vis spectroscopy. To determine the direct bandgap E_g of the samples, Tauc plots were constructed using the relation $(\alpha hv)^2 = C(hv - E_g)$ where α is the absorption coefficient, C is a constant, and hv represents the photon energy. This method, widely applied for estimating optical bandgaps in semiconducting materials, allowed for the calculation of the bandgaps [33].

As shown in Figure 6, the linear portion of the Tauc plot, which corresponds to the absorption edge, was extrapolated to the x-axis to obtain the direct bandgap values. The white HAp powder has a bandgap of 3.99 eV, while the gray powder exhibits a slightly lower bandgap of 3.87 eV. These differences can be attributed to surface properties, as the XRPD and FTIR analyses show

no significant differences in the bulk structure of the powders. The higher bandgap of the white powder aligns with its reflective nature, while the lower bandgap of the gray powder suggests greater absorption of visible light, likely due to surface effects.

Although HAp is typically considered an insulator with a bandgap in the 5–6 eV range, the observed values of 3.99 eV and 3.87 eV fall within a range that indicates possible semiconducting behavior. Bandgap variations reported in the literature can be attributed to the presence of defects and the choice of theoretical methods for bandgap calculations.

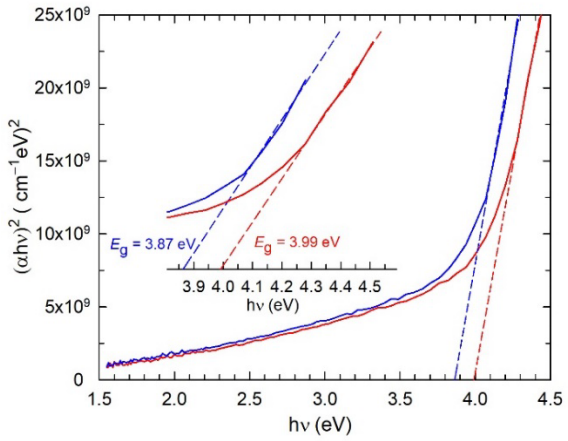

Figure 6. Tauc plot showing the relationship between $(\alpha h\nu)^2$ and photon energy ($h\nu$) for the white and gray hydroxyapatite (HAp) powders. α represents the absorption coefficient. Linear fitting was applied to the absorption edge region, and the extrapolation of the fitted lines to the *x*-axis reveals the direct bandgap (E_g) values. The white powder shows a bandgap of 3.99 eV (red line), while the gray powder has a bandgap of 3.87 eV (blue line). The inset highlights the extrapolation area, illustrating the slight bandgap difference

For example, Rosenman et al. used photoluminescence (PL) and surface photovoltage spectroscopy to study HAp and determined a bandgap of 3.95 eV from the PL spectra. They also determined E_g as 3.94 eV from the contact potential difference (DCPD) curves treatment method [15], consistent with our findings. The comparison between DCPD and PL spectra in [15] demonstrates that the energy levels of electron-hole states obtained from the two spectroscopy techniques are remarkably similar.

This suggests that all HAp samples share an identical electron-hole state structure, comprising five bulk states and one surface state. It is proposed that these deep electron (hole) charged states could be a key factor contributing to the high bioactivity observed in HAp nanoceramics. In contrast, theoretical studies based on density functional theory (DFT) often predict larger bandgap values, ranging from 4.5 to 5.4 eV for HAp, even higher values for defect-free samples [16-18].

It is important to consider the level of defects in HAp, as defect-free HAp is transparent to visible light, with electronic excitations only occurring for photon energies greater than 6 eV. Therefore, accurately determining the fundamental properties of HAp—such as its crystalline structure, phonon dispersion, electronic band structure, dielectric response, and electronic band gap—with minimal error margins is essential for a reliable evaluation of both spectroscopic and theoretical results [19].

Previous studies have demonstrated that doping, as well as the presence of defects and vacancies, can lower the E_g of HAp. For example, the optical bandgap of HAp/TiO_2 composite thin films was found to decrease from 4.1 eV to 3.8 eV with varying dipping cycles [20]. Another study, which combined experimental and theoretical approaches, examined the impact of Ti substitution in HAp on the bandgap. Diffuse reflectance spectroscopy revealed optical bandgap values of 3.65 eV for Ti-HAp, greater than 6 eV for pure HAp, and 3.27 eV for TiO_2. However, bandgaps calculated using DFT yielded lower values, specifically 2.74 eV for Ti-HAp, 4.95 eV for HAp, and 2.23 eV for TiO_2 [21].

A first-principles study on the optoelectronic properties and defect levels in HAp found that donor and acceptor transitions calculated with semi-local DFT differed from those obtained using hybrid-DFT by nearly 2 eV. This large discrepancy underscores the importance of using high-precision methods to describe electron-electron interactions when calculating electronic and optical transitions in HAp defects. Accurate determination of electronic states requires high-quality computational approaches [19].

In this study, the observed bandgap reduction may be attributed to surface effects, oxygen vacancies, or trace impurities introduced during calcination. The presence of the Mg-whitlockite phase could also contribute to the bandgap narrowing, as previous research suggests that defects and impurities significantly influence the bandgap of HAp. Magnesium substitution in whitlockite can lead to lattice distortions and defects, such as oxygen vacancies, which may introduce localized energy states within the bandgap.

These changes could alter the electronic structure and reduce the bandgap. While these observations point towards the potential for semiconducting properties in the modified HAp, further research is required to confirm this behavior and fully understand the influence of the Mg-whitlockite phase, along with other surface effects, on the material's electronic properties.

4. Discussion

This study examines how air exposure during calcination affects the optical and structural properties of hydroxyapatite. While the white and gray powders show distinct color differences, structural analysis confirms that both crystallize in the hexagonal HAp structure with a minor Mg-whitlockite impurity. This indicates that varying calcination conditions do not alter the bulk composition. The Rietveld refinement verified the crystalline structure remained consistent in both powders. The color differences between the white and gray powders are most probably due to surface oxidation occurring during calcination. SEM analysis revealed slight differences in particle morphology, with the white powder displaying a smoother surface than the gray powder. However, these variations are confined to the surface, as no significant deviations in bulk structure were detected. FTIR spectra further confirmed the presence of characteristic phosphate and hydroxyl groups in both powders, indicating that the fundamental chemical structure of HAp was preserved. Additionally, the consistent Ca/P ratios across both powders suggest that the calcination process did not affect the stoichiometric composition, reinforcing the conclusion that the observed color and bandgap differences are surface-driven rather than due to changes in the bulk structure.
Regarding phase composition, both this study and previous investigation [14] confirmed that HAp is the primary phase, with a minor Mg-whitlockite impurity present. However, the study on Nile tilapia scales identified biphasic calcium phosphates, specifically HAp and β-tricalcium phosphate, at higher calcination temperatures [13]. These discrepancies may arise from differences in the source material or the calcination conditions, which can impact the resulting phase composition.

When comparing optical properties, the bandgap values obtained in this study—3.99 eV for the white powder and 3.87 eV for the gray powder—are lower than the 5.5 eV reported in [13] for the white powder obtained after boiling pre-treatment and calcination at 800°C. The same study also reported two bandgap values, 2.87 eV and 3.97 eV, for the blue powder obtained from dry fish scales without pre-treatment, which was calcined at 800°C [13]. These variations in bandgap values likely due to the differences in sample preparation and elemental composition. For example, the tilapia study linked the blue color of dry samples (which lacked boiling pre-treatment) to higher concentrations of Na, Cl, S, and Mn. In contrast, our results suggest that surface effects, particularly air exposure during calcination, are key factors driving the observed color and bandgap differences between the white and gray powders rather than the structural variations in the bulk. This comparison reinforces the significant role that surface conditions, such as air exposure and calcination environment, have on the optical properties of HAp, even when the bulk structure remains mostly unaffected. The difference in the electronic states of HAp between the surface and bulk, as highlighted in [15], further supports this conclusion.

Although the white and gray powders show noticeable color differences, XRPD, FTIR, and SEM analyses reveal no major variations in their bulk crystal structures. This suggests that the color differences are surface-related rather than due to changes in the core crystalline properties. The white color in the outer layers of the calcined scales is likely due to full air exposure, allowing

for complete oxidation and the removal of organic matter. In contrast, the inner gray/black layers, shielded from direct air exposure, may retain carbon residues from incomplete combustion of organic materials like collagen. This could explain the color contrast between the two layers. Localized temperature variations during calcination may also contribute, with the outer layers reaching higher temperatures, ensuring complete decomposition of organic matter, while the inner layers, lacking sufficient air exposure, experience incomplete combustion, leading to the gray hue [34].

The elemental composition of HAp powder obtained from the same fish scales and calcined at 800 °C for 2 hours has been previously analyzed using EDS spectroscopy [14]. The results confirmed that, after calcination, the major elements were calcium, phosphorus, and oxygen, with minor contributions from other trace elements such as magnesium and sodium. However, in the earlier study [14], all the calcined scales were combined, causing the white fraction to be masked by the gray fraction, which yielded an overall gray appearance. Only through the controlled separation of fully exposed and partially shielded scales in the present study was the role of air exposure in color formation definitively identified. In the earlier work, the gray-colored HAp powder exhibited approximately 3.8% residual carbon, indicating that some organic remnants remained in the sample—possibly attributable to reduced air contact during calcination [14].

While the lab-based X-ray diffraction provides useful insights into the bulk crystal structure, it is limited in detecting fine details like oxygen vacancies or other surface defects. High-resolution methods, such as synchrotron X-ray or neutron diffraction, would offer better sensitivity to light elements like oxygen and could give a clearer picture of structural defects responsible for the observed bandgap narrowing. These advanced techniques could help confirm whether oxygen deficiencies or other defects are influencing the surface properties, giving us a deeper understanding of the material's electronic and optical behavior.

5. Conclusion

This research highlights the critical impact of surface effects on the optical properties of hydroxyapatite (HAp) powders extracted from fish scales. Structural analysis confirms that both the white and gray powders crystallize in the hexagonal HAp structure along with a minor Mg-whitlockite impurity, indicating that the bulk crystalline structure remains unchanged despite variations in air exposure. Although the gray powder may retain slightly more residual carbon, Rietveld refinements confirm no significant deviation in space group or lattice parameters. These results suggest that air exposure primarily affects surface properties—particularly those linked to optical characteristics—rather than inducing detectable changes in the bulk structure of the HAp. UV-Vis spectroscopy shows bandgap values of 3.99 eV for the white powder and 3.87 eV for the gray powder. These values, while lower than those typically reported for defect-free HAp (5–6 eV), align with previously reported bandgaps for HAp containing surface defects. This suggests possible semiconducting behavior in the extracted HAp, influenced by surface phenomena rather than changes in the bulk structure. These findings can contribute to a deeper understanding of how calcination conditions impact the optical, surface and structural properties of biogenic HAp, which has important implications for its use in biomedical applications and environmental remediation, where surface characteristics play a critical role in performance.

Article Information Form

Acknowledgments
The author would like to express sincere thanks to Kocamanlar Seafood for providing the fish scales used in this study and Tabii Soğuk Hava Depoculuk Limited Co. for their financial support.

Funding
The author has no received any financial support for the research, authorship or publication of this study.

The Declaration of Conflict of Interest/ Common Interest

No conflict of interest or common interest has been declared by the author.

The Declaration of Ethics Committee Approval

This study does not require ethics committee permission or any special permission.

The Declaration of Research and Publication Ethics

The author of the paper declares that she complies with the scientific, ethical and quotation rules of SAUJS in all processes of the paper and affirms that no falsification has been made on the data collected. In addition, the author declares that Sakarya University Journal of Science and its editorial board have no responsibility for any ethical violations that may be encountered, and that this study has not been evaluated in any academic publication environment other than Sakarya University Journal of Science.

References

[1] P. W. Brown, B. Constantz, Hydroxyapatite and related materials, USA:CRC press Boca Raton, 1994.

[2] H. Cölfen, "A crystal-clear view," Nature Materials, vol. 9, no. 12, pp. 960–961, 2010.

[3] S. F. Jackson, J. T. Randall, "The fine structure of bone," Nature, vol. 178, no. 4537, p. 798, 1956.

[4] R. Murugan, S. Ramakrishna, "Development of nanocomposites for bone grafting," Composites Science and Technology, vol. 65, no. 15, pp. 2385–2406, 2005.

[5] N. Eliaz, N. Metoki, "Calcium phosphate bioceramics: A review of their history, structure, properties, coating technologies and biomedical applications.," Materials (Basel, Switzerland), vol. 10, no. 4, 2017.

[6] A. S. Posner, A. Perloff, A. F. Diorio, "Refinement of the hydroxyapatite structure," Acta Crystallogr., vol. 11, no. 4, pp. 308–309, 1958.

[7] J. C. Elliott, P. E. Mackie, R. A. Young, "Monoclinic hydroxyapatite," Science, vol. 180, no. 4090, pp. 1055–1057, 1973.

[8] G. Ma, X. Y. Liu, "Hydroxyapatite: hexagonal or monoclinic?," Crystal Growth & Design, vol. 9, no. 7, pp. 2991–2994, Jul. 2009.

[9] M. Sadat-Shojai, M.-T. Khorasani, E. Dinpanah-Khoshdargi, A. Jamshidi, "Synthesis methods for nanosized hydroxyapatite with diverse structures," Acta Biomaterials, vol. 9, no. 8, pp. 7591–7621, 2013.

[10] P. Arokiasamy, M. M. A. B Abdullah, S. Z. Abd Rahim, S. Luhar, A. V. Sandu, N. H. Jamil, M. Nabiałek, "Synthesis methods of hydroxyapatite from natural sources: A review," Ceramics International, vol. 48, no. 11, pp. 14959–14979, 2022.

[11] N. A. S. Mohd Pu'ad, P. Koshy, H. Z. Abdullah, M. I. Idris, T. C. Lee, "Syntheses of hydroxyapatite from natural sources," Heliyon, vol. 5, no. 5, p. e01588, 2019.

[12] V.-R. Maria, D. A. Navarrete, D. Arcos, Biomimetic Nanoceramics in Clinical Use: From Materials to Applications. Cambridge: Royal Society of Chemistry, 2008.

[13] T. Eknapakul, S. Kuimalee, W. Sailuam, S. Daengsakul, N. Tanapongpisit, P. Laohana, W. Saenrang, A. Bootchanont, A. Khamkongkaeo, R. Yimnirun, "Impacts of pre-treatment methods on the morphology, crystal structure, and defects formation of hydroxyapatite extracted from Nile tilapia scales," RSC Advances, vol. 14, no. 7, pp. 4614–4622, 2024.

[14] H. E. Okur, "Rietveld refinement-based structural analysis of biogenic hydroxyapatite and its PVA composite for dye removal," Mater. Today Commun., vol. 43, p. 111723, 2025

[15] G. Rosenman, D. Aronov, L. Oster, "Photoluminescence and surface photovoltage spectroscopy studies of hydroxyapatite nano-Bio-ceramics," Journal of Luminescence, vol. 122–123, pp. 936–938, 2007.

[16] K. Matsunaga, A. Kuwabara, "First-principles study of vacancy formation in hydroxyapatite," Physical Review B, vol. 75, no. 1, p. 14102, 2007.

[17] L. Calderin, M. J. Stott, A. Rubio, "Electronic and crystallographic structure of apatites," Physical Review. B, vol. 67, no. 13, p. 134106, 2003.

[18] P. Rulis, L. Ouyang, W. Y. Ching, "Electronic structure and bonding in calcium apatite crystals: Hydroxyapatite, fluorapatite, chlorapatite, and bromapatite," Physical Review B, vol. 70, no. 15, p. 155104, 2004.

[19] L. A. Avakyan, E. V Paramonova, J. Coutinho, S. Oberg, V. S. Bystrov, L. A. Bugaev, "Optoelectronics and defect levels in hydroxyapatite by first-principles," Journal of Chemical Physics, vol. 148, no. 15, 2018.

[20] K. Kaviyarasu, A. Mariappan, K. Neyvasagam, A. Ayeshamariam, P. Pandi, R. R. Palanichamy, C. Gopinathan, G. T. Mola, M. Maaza "Photocatalytic performance and antimicrobial activities of HAp-TiO_2 nanocomposite thin films by sol-gel method," Surfaces and Interfaces, vol. 6, pp. 247–255, 2017.

[21] M. Tsukada, M. Wakamura, N. Yoshida, T. Watanabe, "Band gap and photocatalytic properties of Ti-substituted hydroxyapatite: Comparison with anatase-TiO_2," J. Mol. Catal. A-Chemical, vol. 338, no. 1–2, pp. 18–23, 2011.

[22] V. S. Bystrov, E. Paramonova, L. Avakyan, J. Coutinho, N. Bulina, "Simulation and computer study of structures and physical properties of hydroxyapatite with various defects,"Nanomaterials" vol. 11, no. 10, 2021,

[23] V. S. Bystrov, J. Coutinho, A. V. Bystrova, D. Y. Dekhtyar, R. C. Pullar, A. Poronin, A. Palcevskis, A. Dindune, B. Alkan, B. C. Durucan, E. V. Paramonova, "Computational study of hydroxyapatite structures, properties and defects," J. Phys. D. Appl. Phys., vol. 48, no. 19, pp. 195302, 2015

[24] R. Rial, M. Gonzalez-Durruthy, Z. Liu, J. M. Ruso, "Advanced materials based on nanosized hydroxyapatite," Molecules, vol. 26, no. 11, 2021

[25] A. C. Larson, R. Von Dreele, "General Structure Analysis System (GSAS)," Los Alamos National. Laboratory Rep. LAUR, pp. 86–748, 2004.

[26] P. Thompson, D. E. Cox, J. B. Hastings, "Rietveld refinement of Debye-Scherrer synchrotron X-ray data from A1203," Journal of Applied Crystallography, vol. 20, no. 2, pp. 79–83, 1987.

[27] J. Laugier, B. Bochu, "LMGP-suite of programs for the interpretation of X-ray experiments." ENSP/Laboratoire des Matériaux et du Génie Physique, 1999.

[28] K. Sudarsanan, R. A. Young, "Significant precision in crystal structural details. Holly Springs hydroxyapatite," Acta Crystallographica Section B, vol. 25, no. 8, pp. 1534–1543, 1969.

[29] R. Gopal, C. Calvo, J. Ito, W. K. Sabine, "Crystal structure of synthetic Mg-Whitlockite, $Ca_{18}Mg_2H_2(PO_4)_{14}$," Canadian Journal of Chemistry, vol. 52, no. 7, pp. 1155–1164, 1974.

[30] E. Hosseinzadeh, M. Davarpanah, N. H. Nemati, S. A. Tavakoli, "Fabrication of a hard tissue replacement using natural

hydroxyapatite derived from bovine bones by thermal decomposition method," International Journal of Organ Transplantation Medicine, vol. 5, no. 1, pp. 23–31, 2014.

[31] R. X. Sun, Y. Lv, Y. R. Niu, X. H. Zhao, D. S. Cao, J. Tang, J., K. Z. Chen, "Physicochemical and biological properties of bovine-derived porous hydroxyapatite/collagen composite and its hydroxyapatite powders," Ceram. Int., vol. 43, no. 18, pp. 16792–16798, 2017.

[32] J. M. Stutman, J. D. Termine, A. S. Posner, "Vibrational spectra and structure of the phosphate ion in some calcium phosphates," Trans. N. Y. Academic Science, vol. 27, no. 6 Series II, pp. 669–675, 1965.

[33] J. Tauc, "Optical Properties and Electronic Structure of Amorphous Semiconductors," in Optical Properties of Solids, S. Nudelman and S. S. Mitra, Eds., Boston, MA: Springer US, 1969, pp. 123–136.

[34] M. Šupová, "Problems associated with the assessment of organic impurities in bioapatites isolated from animal sources: A review," Journal of the Australian Ceramic Society, vol. 58, no. 1, pp. 227–247, 2022.